Journal of the Mechanical Behavior of Biomedical Materials 74 (2017) 428–437

Contents lists available at ScienceDirect

Journal of the Mechanical Behavior of Biomedical Materials

journal homepage: www.elsevier.com/locate/jmbbm

Elastic properties and strain-to-crack-initiation of calcium phosphate bone cements: Revelations of a high-resolution measurement technique

Ingrid Ajaxon[a,1], Alice Acciaioli[b,1], Giacomo Lionello[b], Maria-Pau Ginebra[c], Caroline Öhman-Mägi[a], Massimiliano Baleani[b], Cecilia Persson[a,*]

[a] Materials in Medicine Group, Division of Applied Materials Science, Department of Engineering Sciences, Uppsala University, Box 534, 751 21 Uppsala, Sweden
[b] Istituto Ortopedico Rizzoli, Laboratorio di Tecnologia Medica, Via di Barbiano 1/10, 40136 Bologna, Italy
[c] Biomaterials, Biomechanics and Tissue Engineering Group, Dept. of Materials Science and Metallurgy, Technical University of Catalonia (UPC), Av. Eduard Maristany 10-14, 08019 Barcelona, Spain

ARTICLE INFO

Keywords:
Bone cement
Calcium phosphate
Brushite
Apatite
Monetite
Elastic modulus
Poisson's ratio
Mechanical properties

ABSTRACT

Calcium phosphate cements (CPCs) should ideally have mechanical properties similar to those of the bone tissue the material is used to replace or repair. Usually, the compressive strength of the CPCs is reported and, more rarely, the elastic modulus. Conversely, scarce or no data are available on Poisson's ratio and strain-to-crack-initiation. This is unfortunate, as data on the elastic response is key to, *e.g.*, numerical model accuracy. In this study, the compressive behaviour of brushite, monetite and apatite cements was fully characterised. Measurement of the surface strains was done using a digital image correlation (DIC) technique, and compared to results obtained with the commonly used built-in displacement measurement of the materials testers. The collected data showed that the use of fixed compression platens, as opposed to spherically seated ones, may in some cases underestimate the compressive strength by up to 40%. Also, the built-in measurements may underestimate the elastic modulus by up to 62% as compared to DIC measurements. Using DIC, the brushite cement was found to be much stiffer (24.3 ± 2.3 GPa) than the apatite (13.5 ± 1.6 GPa) and monetite (7.1 ± 1.0 GPa) cements, and elastic moduli were inversely related to the porosity of the materials. Poisson's ratio was determined to be 0.26 ± 0.02 for brushite, 0.21 ± 0.02 for apatite and 0.20 ± 0.03 for monetite. All investigated CPCs showed low strain-to-crack-initiation (0.17–0.19%). In summary, the elastic modulus of CPCs is substantially higher than previously reported and it is concluded that an accurate procedure is a prerequisite in order to properly compare the mechanical properties of different CPC formulations. It is recommended to use spherically seated platens and measuring the strain at a relevant resolution and on the specimen surface.

1. Introduction

Calcium phosphate cements (CPCs) have gained a great deal of attention since they were first introduced in the beginning of the 1980s, due to their chemical similarity to the mineral content of bone (Bohner et al., 2005; Dorozhkin, 2010). They are biocompatible, osteoconductive, and can be made injectable. The main application of CPCs is to fill bone voids, but they can also be used together with metallic devices in fracture stabilization, especially in patients with low-quality bone (Bajammal, 2008; Larsson and Bauer, 2002).

Ideally, the CPCs should have mechanical properties matching those of the bone tissue the material is used to replace or repair (Tamimi et al., 2012). However, the strength and stiffness of the osseous tissue can vary substantially, not only depending on anatomical site and within different regions of the same bony site, but also among individuals, with age, sex, activity level and, due to different pathologies (Pruitt and Chakravartula, 2011). Cortical bone is much stronger and stiffer compared to trabecular bone; literature values for compressive strength, yield strain, elastic modulus and Poisson's ratio for cortical and trabecular bone can be found in Table 1.

Some of the main limitations of CPCs are their brittleness and their poor resistance to tensile forces. Moreover, as for most porous ceramic materials tensile tests are difficult to set-up for CPCs (Pittet and Lemaître, 2000). Indeed, the most common mechanical assessment of CPCs is quasi-static compression testing (Ajaxon and Persson, 2017; Tamimi et al., 2012; Zhang et al., 2014), which is not dependent on fixation and specimens are easy to prepare.

It has been demonstrated that the compressive strength varies

* Correspondence to: The Ångström Laboratory, Department of Engineering Sciences, Division of Applied Materials Science, Box 534, SE-751 21 Uppsala, Sweden.
E-mail address: cecilia.persson@angstrom.uu.se (C. Persson).
[1] These authors contributed equally to the work.

http://dx.doi.org/10.1016/j.jmbbm.2017.06.023
Received 31 March 2017; Received in revised form 16 June 2017; Accepted 20 June 2017
Available online 21 June 2017

Table 1
Ranges reported in the literature for mechanical properties of cortical and trabecular bone, as well as three different types of calcium phosphate cements. All reported values are for wet (or moist) specimens, if not otherwise indicated. Tabulated values of yield strain, elastic modulus and Poisson's ratio for bone were determined using external extensometers.

	Ultimate compressive strength [MPa]	Yield strain [%]	Elastic modulus [GPa]	Poisson's ratio
Cortical bone	95–230 (Öhman et al., 2011; Kaneko et al., 2003)	0.8–1.2 (Kaneko et al., 2003; Öhman et al., 2011)	9–25 (Helgason et al., 2008; Öhman et al., 2011)	0.46–0.58 (Keaveny and Hayes, 1993; Reilly and Burstein, 1975)
Trabecular bone	1–30 (Kopperdahl and Keaveny, 1998; Perilli et al., 2008)	0.6–1.2 (Bayraktar et al., 2004; Bevill et al., 2009; Morgan and Keaveny, 2001; Kopperdahl and Keaveny, 1998)	0.01–5 (Helgason et al., 2008: Bevill et al., 2009; Morgan and Keaveny, 2001; Kopperdahl and Keaveny, 1998)	0.06–0.95 (Keaveny and Hayes, 1993)
Brushite	0.4–74 (Ajaxon and Persson, 2017)	Not reported	2–8 (Ajaxon and Persson, 2017)	Not reported
Monetite	2–14 (Åberg et al., 2010; Åberg et al., 2013)	Not reported	0.4–1 (Boroujeni et al., 2013, Cama et al., 2013)	Not reported
Apatite	0.5–101 (Barralet et al., 2003; Gbureck et al., 2005; Zhang et al., 2014; Ginebra, 2008)	2–2.4[a] (Habraken et al., 2008; Lian et al., 2008)	0.4–8 (Liu et al., 2014; Xu et al., 2010; Rajzer et al., 2016)	0.19 (Rajzer et al., 2016)

[a] Determined for dry specimens.

greatly between different types of CPCs (Table 1), due to differences in chemical composition, particle size of starting powders, additives, liquid to powder (L/P) ratio, sample preparation, resulting porosity, storage and testing conditions (*e.g.*, testing dry or wet cements) (Ajaxon and Persson, 2017; Tamimi et al., 2012; Zhang et al., 2014; Espanol et al., 2009). Commercially available CPCs usually have apatite or brushite (dicalcium phosphate dihydrate) as the main resultant phase (Bohner et al., 2005). Apatite cements have been extensively investigated due to their similarity to bone mineral and have traditionally been reported to be stronger than brushite cements (Ajaxon and Persson, 2017; Zhang et al., 2014). However, recent advances show that brushite cements can have as high strength as apatite cements (Barralet et al., 2003; Hofmann et al., 2009; Unosson and Engqvist, 2014; Zhang et al., 2014). Conversely, the strength of monetite (dicalcium phosphate anhydrous) cements is generally lower, chiefly due to their higher porosity (Åberg et al., 2010; Habibovic et al., 2008). Clinically, brushite and monetite cements may have advantages over apatite cements in terms of faster *in vivo* resorption (Apelt et al., 2004; Bohner et al., 2012; Tamimi et al., 2012), and some have shown osteoinductive effects (Engstrand et al., 2015; 2014; Habibovic et al., 2008).

Literature values of the elastic modulus of CPCs are scarce (Table 1). More importantly, values reported in the literature may be substantially underestimated. In fact, either the elastic modulus has been calculated from the linear part of the stress-strain curve with the displacement of the platens obtained directly from the built-in system of the materials testing machine, or the method is not specified at all (Ajaxon and Persson, 2017; Boroujeni et al., 2013; Cama et al., 2013; Xu et al., 2010). The platen technique, where the strain is taken from the displacement of the compression platens, is a simple method, but it suffers from low accuracy for brittle materials, as has previously been reported for mechanical testing of calcium sulphate dihydrate cements (Koh et al., 2014).

There is therefore a scarcity of accurate values of the elastic modulus of CPCs in the literature, as well as very limited data on their Poisson's ratio and strain to failure (available only for some apatite cements, Table 1). An accurate knowledge of these material parameters is crucial in material development aimed at comparing the properties of different formulations or in computational models aimed to predict the material behaviour in simulated clinical scenarios. To improve accuracy, material deformation can be measured on the surface of the specimen, thereby eliminating end artefacts (Koh et al., 2014). However, contact extensometers need to be mounted directly onto the specimen surface. Therefore, there is a high risk that knife edges induce flaws on the specimen surface, which the brittle CPCs are very sensitive to. Besides, adhesives used to apply strain gauges may penetrate into pores on the cement surface, affecting the material's mechanical response. Moreover, CPCs exhibit very small deformations before failure, making it difficult to accurately determine the deformation using optical methods (Siebert et al., 2007). Recently, it has been demonstrated that the digital image correlation (DIC) technique can accurately measure small-magnitude ($< 0.1\%$) homogeneous strain fields (Acciaioli et al., Submitted for publication) indicating that the DIC technique is suitable to accurately determine also the small strains that CPCs undergo during compressive testing.

The aim of this study was to determine the compressive behaviour of different formulations of injectable CPCs using the DIC technique, with a focus on the underexplored elastic properties. Additionally, the compressive behaviour determined using different experimental procedures was compared.

2. Materials and methods

2.1. Cement preparation

The mechanical properties of three different types of calcium phosphate cements were investigated: a brushite cement, a monetite cement and an apatite cement.

2.1.1. Brushite cement preparation

The powder phase of the brushite cement consisted of 45:55 mol% monocalcium phosphate monohydrate (MCPM; Scharlau, Sentmenat, Spain): beta-tricalcium phosphate (ß-TCP; Sigma-Aldrich, St. Louis, MO, USA). The as-received MCPM powder was first sieved and only particle sizes below 75 µm was used. The two powders were mixed with 1 wt% disodium dihydrogen pyrophosphate (Sigma-Aldrich, St. Louis, MO, USA), acting as a retardant (Unosson, 2014). The liquid phase consisted of a 0.5 M citric acid solution (Sigma-Aldrich, St. Louis, MO, USA). The powder and liquid phases were mixed at an L/P-ratio of 0.22 ml/g for 1 min in a mechanical mixing device (Cap Vibrator Ivoclar Vivadent AG, Schaan, Liechtenstein).

The cement paste was moulded and specimens were left to set for 24 h in phosphate buffered saline (PBS; Sigma-Aldrich, St. Louis, MO, USA; containing 0.01 M phosphate buffer, 0.0027 M potassium chloride and 0.137 M sodium chloride, pH 7.4) at 37 °C to achieve full setting (Unosson and Engqvist, 2014).

2.1.2. Monetite cement preparation

The powder phase of the monetite cement consisted of 45:55 mol% MCPM (Scharlau, Sentmenat, Spain): ß-TCP (Sigma-Aldrich, St. Louis, MO, USA). The powder was mixed with glycerol (Sigma-Aldrich, St. Louis, MO, USA) at an L/P ratio of 0.26 ml/g for 180 s. The cement was then injected into moulds, which were immersed in deionized water during 72 h to achieve full setting by diffusion of water into the cement. The cement specimens were subsequently dried in air for 24 h and then

autoclaved (120 °C for 20 min). Specimens were soaked in PBS for 24 h at 37 °C, before mechanical testing.

2.1.3. Apatite cement preparation

Alpha-tricalcium phosphate (α-TCP) was used as the powder phase for the apatite cement. The preparation of α-TCP has been described elsewhere (Espanol et al., 2009). Briefly, calcium hydrogen phosphate (Sigma-Aldrich, St. Louis, MO, USA) and calcium carbonate (Sigma-Aldrich, St. Louis, MO, USA) were mixed in appropriate amounts, heated at 1400 °C for 15 h followed by quenching in air and then milled to a coarse powder (median particle size 5.2 μm). Precipitated hydroxyapatite (2 wt%; Alco, Akron, OH, USA) was added as seed particles, which act as crystal nuclei (Espanol et al., 2009). The liquid phase was a 2.5 wt% sodium hydrogen phosphate solution (Sigma- Aldrich, St. Louis, MO, USA), added to accelerate the setting reaction (Espanol et al., 2009). An L/P ratio of 0.35 ml/g was used and the two phases were machine mixed for 1 min. The paste was moulded and specimens were left to set for 7 days in PBS at 37 °C to achieve full setting (Ginebra et al., 2004).

2.1.4. Specimen geometries

There is no specific standard available concerning mechanical testing of ceramic cements used as biomaterials. Therefore, recommendations of specimen dimensions in other standards were referred to, when possible, when selecting specimen geometry.

The compressive strength was determined testing cylindrical samples according to standards for acrylic cements (ASTM, 2008; ISO, 2002), which are commonly used for compression testing of CPCs (Ajaxon and Persson, 2017). The elastic properties of the material, *i.e.*, elastic modulus and Poisson's ratio, were also measured under uniaxial compressive stress. Due to the brittleness of CPCs, it is not possible to determine these properties under tensile conditions, as recommended in the available standard for plastics (ASTM, 2014). Hence, a squared cross-section (with rounded edges) parallelepiped geometry, whose length was twice its width, was chosen according to the standard for compressive testing of plastics (ASTM, 2015). A parallelepiped geometry was chosen instead of a cylindrical shape because flat specimen surfaces are necessary to measure axial and transverse strain simultaneously (used to calculate Poisson's ratio). The two different geometries of specimens used in this study are illustrated in Fig. 1.

2.2. Cement compression

After setting, the specimens were wet polished using SiC paper, to achieve plane parallel end surfaces and final heights according to Fig. 1.

For each cement type, cylindrical specimens were randomly assigned to two different groups and monotonic compression tests of the specimens were performed using two different axially loaded testing frames. The first group was loaded to failure using a universal testing machine (AGS-X, Shimadzu, Kyoto, Japan) equipped with fixed compression platens (FP), see Fig. 2a. The FP displacement was measured by an optical encoder with an accuracy of ± 0.01 mm in the used range. The other group was loaded to failure using a universal testing machine (Mod.8502, Instron, Norwood, MA, USA) equipped with spherically seated compression platens (SSP), allowing for compensation of misalignments of the specimens' end surfaces, see Fig. 2b. The SSP displacement was measured by a linear variable differential transducer (LVDT) with an accuracy of ± 0.01 mm in the used range. In the latter series one side of the specimen was monitored by means of a DIC system (Aramis 5 M, GOM mbH, Braunschweig, Germany), whose cameras were arranged stereoscopically for 3D measurement, to measure longitudinal strain, see Fig. 2b.

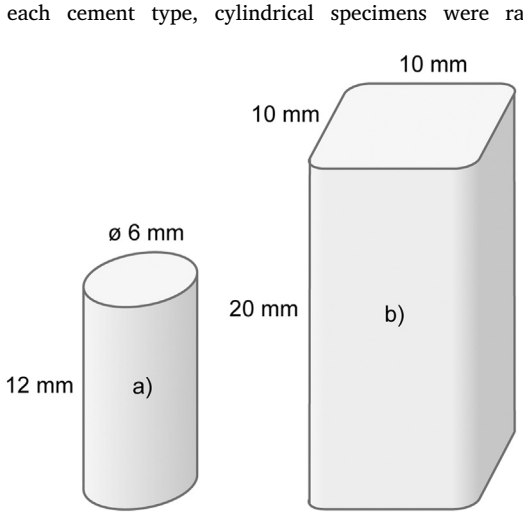

Fig. 1. Specimen geometries used in this study: a) cylindrical specimen and b) rectangular parallelepiped specimen.

To determine the elastic modulus and Poisson's ratio, the parallelepiped specimens were loaded in compression using the set-up with the SSP. However, in this series the two cameras of the DIC system monitored two opposite sides of the specimens simultaneously, *i.e.*, they were arranged for 2D measurement, see Fig. 2c.

In both configurations, the DIC system was setup to acquire images under experimental conditions optimized to maximize pixel size and depth-of-field while assuring adequate surface illumination. Prior to testing, a speckle pattern was created on the surface of the specimens, which underwent DIC measurements. A detailed description of the procedure can be found elsewhere (Acciaioli et al., Submitted for publication). Briefly, the pixel size was calculated considering the camera resolution and the current measuring-window size. An algorithm, preliminary defined for the used airbrush (Iwata HP-CH, 0.3 mm nozzle, Anest Iwata Europe S.r.l., Torino, Italy) following the approach described by Lionello and Cristofolini (Lionello and Cristofolini, 2014), was used to determine airbrush settings to achieve the desired speckle size of 3–5 pixels (Sutton et al., 2009; Zhou, 2001). A trained operator (A.A.) sprayed black paint with the airbrush onto the specimen to obtain the recommended speckle-to-surface area ratio of 42–50% (Carter and Uchic, 2015). Achieved speckle patterns, evaluated using a mathematical morphology technique (Lecompte et al., 2006; Lionello et al., 2014) fulfilled the above-described requirements.

In all above-mentioned tests, the specimens were loaded parallel to their longitudinal axis and tests were performed using a cross-head speed of 1 mm min^{-1}. The brushite and apatite cements were kept wet (brushite soaked in isopropanol, apatite in PBS (Ajaxon et al., 2015)) until they were tested. The monetite cements were soaked in PBS for 24 h at 37 °C, before mechanical testing.

Crack initiation resistance (σ_{CIR}) was defined as the stress value calculated for the first drop in load. This load drop appeared due to internal defects and surface irregularities and could sometimes be observed as chipping, but not complete specimen failure. The ultimate compressive strength (σ_{UCS}) was the maximum stress value measured during testing and corresponded to complete specimen (brittle) failure.

Elastic modulus was calculated as the slope of the linear part of the stress-strain curve. Three different methods were used to calculate strain values: (1) using the machine-measured displacement of the FP (cylindrical specimens); (2) using the machine-measured displacement of the SSP (cylindrical and parallelepiped specimens); (3) using the calculated DIC strain (SSP set-up, parallelepiped specimens). The compliances of both experimental set-ups, *i.e.* using FP and SSP, were taken into account. The DIC strains were obtained averaging the longitudinal strain measured on two opposite specimen surfaces over an area of interest of 8 × 4 mm. A subset of 60 × 60 pixels, experimentally determined as the optimal subset size for the current conditions (Acciaioli et al., Submitted for publication), a 50% overlap ratio (Koohbor et al., 2017) and a 3 × 3 computation size (Eriksen et al., 2010) were used in image-processing to calculate surface strain. Prior to image processing, image pre-selection was carried out checking the

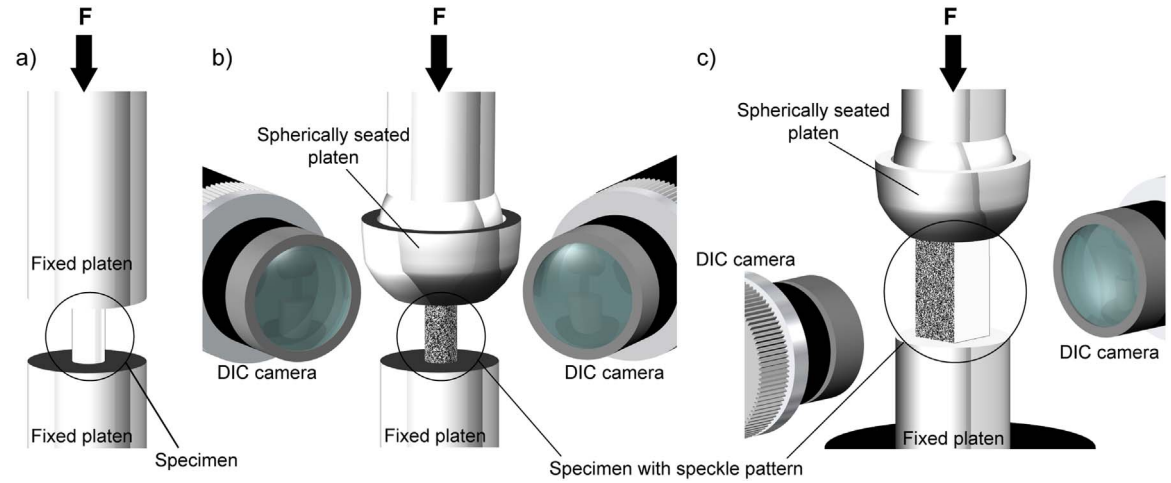

Fig. 2. Schematic of experimental set-up for monotonic compression testing with a) fixed platens (FP), b) spherically seated platens (SSP) and the digital image correlation (DIC) system for 3D measurement and, c) DIC system set-up for 2D measurement.

error in the direction of the calculated strains over the whole area of interest. Images for which 99.7% of the values in all directions differed more than 0.5% from the expected direction – *i.e.* parallel or perpendicular to the loading axis – were discarded. (Acciaioli et al., Submitted for publication).

Poisson's ratio was calculated as the absolute value of the ratio of transverse to longitudinal strain determined by the DIC technique on the parallelepiped specimens. The ratio was calculated for longitudinal strain values in the linear range of the stress-strain curve.

Strain-to-crack-initiation (ε_{CIR}) was defined as the strain measured when the first drop in load was observed (*i.e.*, the strain the material can withstand without damaging). ε_{CIR} was calculated on cylindrical specimens using the same procedure described above except for the area of interest (3 × 4 mm instead of 8 × 4 mm to take into account the different specimen geometry) and image pre-selection (no image pre-selection was carried out due to changes occurring in the strain direction close to failure). Ultimate strain could not be measured due to (i) if chipping occurred on the monitored surface, the DIC system lost tracking of the speckle pattern; and (ii) if a crack occurred in the bulk, the loading situation was different to that expected in areas that the DIC system was measuring on.

2.3. Porosity determination

The porosity of the same brushite cement composition has been evaluated before and found to be 13 ± 2% (Ajaxon et al., 2015). The porosity of the same apatite cement composition has previously been reported to be 38 ± 7% (Canal et al., 2013). The porosity of the monetite cement was determined by water resaturation in the present study, according to the method described by Engstrand Unosson et al. (2015). Briefly, the cement was weighed before and after being immersed in water. Then, the porosity was calculated from the volume of water in all open pores and the apparent volume of the specimen, determined by Archimedes' principle.

2.4. Phase characterization

The phase composition of the prepared brushite, monetite and apatite specimens was analyzed using X-ray diffraction (XRD; D8 Advance, Bruker AXS GmbH, Karlsruhe, Germany). XRD data was collected using a theta-theta setup with Ni-filtered Cu-Kα irradiation, between diffraction angles (2θ) of 5–60°. A step size of 0.02 deg with 0.25 s per step and a sample rotation speed of 80 rpm were used for the analysis. Rietveld refinement, using the BGMN software (version 4.2.22, http://www.bgmn.de) (Bergmann et al., 1998; Taut et al., 1998) with Profex (version 3.1.2, http://profex.doebelin.org) (Doebelin and Kleeberg, 2015) as user interface, was applied to quantify the phase composition, with the reported result being the mean of six measurements per cement type. The repeatability was taken as 2.77 x standard deviation according to ASTM E177-14 (ASTM, 2013; Döbelin, 2015). Crystalline models were taken from PDF# 01-074-0565 (Sudarsanan and Young, 1969) for hydroxyapatite and PDF# 04-010-4348 (Mathew et al., 1977) for α-TCP, PDF# 04-008-8714 (Dickens et al., 1974) for ß-TCP, PDF# 04-013-3344 (Curry and Jones, 1971) for brushite, PDF# 04-009-3876 (Boudin et al., 1993) for beta-calcium pyrophosphate (ß-CPP), and PDF# 04-009-3755 (Dickens et al., 1971) for monetite.

2.5. Statistical evaluation

IBM® SPSS® Statistics (version 22, IBM Corp., Armonk, NY, USA) was used to perform an analysis of variance (ANOVA). Welch's robust test of equality of means and Tamhane's post-hoc test were used since homogeneity of variance could not be confirmed between groups (using Levene's test). A significance level of $\alpha = 0.05$ was used in all above tests.

3. Results

3.1. Cement compression

σ_{UCS} of the three types of cement, determined by compression of the cylindrical specimens using both FP and SSP, are presented in Fig. 3. The three cement formulations behaved differently under compression. The brushite and apatite specimens were found to be significantly stronger than the monetite specimens, regardless of which type of platens that were used ($p < 0.001$). σ_{UCS} of the brushite cement was found to be significantly higher when SSP (56.4 ± 12.0 MPa) were used compared to FP (33.9 ± 8.4 MPa) ($p < 0.001$), whereas both monetite and apatite cements showed no significant difference in σ_{UCS} when tested with FP (12.4 ± 1.8 MPa for monetite and 34.9 ± 7.1 MPa for apatite) and SSP (13.0 ± 1.6 MPa for monetite and 39.1 ± 8.6 MPa for apatite) ($p = 0.95$ and $p = 0.48$ for monetite and apatite, respectively). The brushite cement was found to have a significantly higher σ_{UCS} compared to apatite when SSP were used ($p < 0.001$), whereas when using FP there was no significant difference in σ_{UCS} ($p > 0.999$).

Values of σ_{CIR} and σ_{UCS} of the three types of cement, determined by compression of the cylindrical specimens with SSP, are shown in Fig. 4. σ_{UCS} was not significantly higher than σ_{CIR} for the brushite ($p = 0.24$) and monetite ($p > 0.999$) formulations. Conversely, a significant difference was found between σ_{UCS} and σ_{CIR} values of the apatite cement

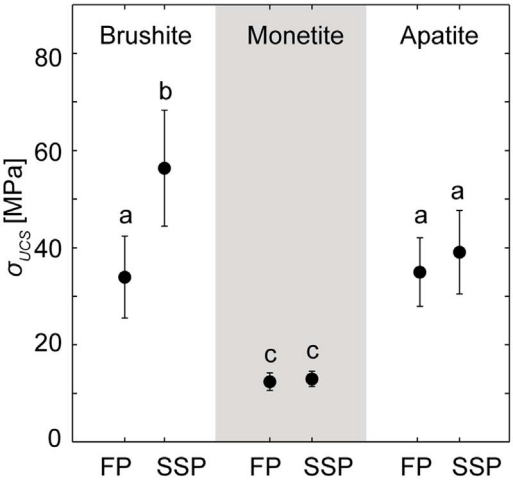

Fig. 3. Mean values of σ_{UCS} for the three types of cements determined from compression testing of cylinders with both FP and SSP (sample size N ≥ 30 for all groups). Error bar shows one standard deviation. Groups with the same letter are not significantly different.

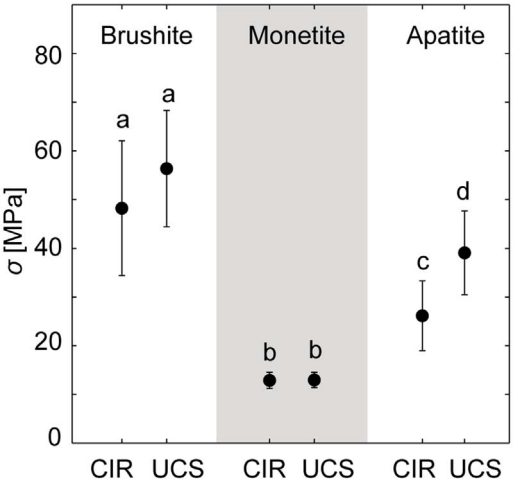

Fig. 4. Mean values of σ_{CIR} and σ_{UCS} for the three types of cements determined from compression testing of cylinders with SSP (sample size N = 30 for all groups). Error bar shows one standard deviation. Groups with the same letter are not significantly different.

($p < 0.001$).

Similarly to the σ_{UCS} values determined using SSP, the brushite cement was found to have a significantly higher σ_{CIR} compared to apatite and monetite ($p < 0.001$), and apatite showed significantly higher σ_{CIR} than monetite ($p < 0.001$).

All three cement formulations showed a brittle behaviour. Additionally, despite the differences observed in σ_{UCS}, there were no significant differences ($p > 0.999$) among the ε_{CIR} values determined for brushite (0.19 ± 0.06%), monetite (0.17 ± 0.03%) and apatite (0.19 ± 0.06%).

The elastic modulus of the three types of cements determined testing cylindrical specimens using FP and SSP, and parallelepiped specimens monitored by the DIC system are shown in Fig. 5. For completeness, also the elastic modulus determined using the SSP displacement of parallelepiped specimens is shown (for each type of cement, there was no significant difference in elastic modulus between specimen geometries, $p \geq 0.3$). The elastic moduli for all three cement formulations followed the same trend: the moduli were significantly lower for platen measurements compared to DIC ($p \leq 0.001$). The DIC-system gave three times higher values compared to FP for the brushite specimens (from 9.2 ± 3.7 GPa to 24.3 ± 2.3 GPa). For monetite and apatite, DIC resulted in almost twice as high moduli compared to FP (from 4.3 ± 0.9 GPa to 7.1 ± 1.0 GPa for monetite and from 8.4 ± 2.5 GPa to 13.5 ± 1.6 GPa for apatite). For the brushite cement, the difference in elastic moduli obtained from FP and SSP was significant ($p < 0.001$), whereas no significant differences were found for monetite ($p \geq 0.3$) and apatite ($p \geq 0.9$).

Comparing between cements, there was a significant difference in moduli obtained from FP between brushite and monetite ($p < 0.001$) and monetite and apatite ($p < 0.001$), whereas the difference between brushite and apatite was not significant ($p > 0.999$). Elastic moduli obtained from SSP and DIC were found to be significantly different among all cement types ($p < 0.001$).

Poisson's ratio, calculated from tests performed with parallelepiped specimens, of brushite, monetite and apatite cement were 0.26 ± 0.02, 0.20 ± 0.03, and 0.21 ± 0.02, respectively. A significant difference in Poisson's ratio was found between brushite and monetite ($p < 0.001$) and between brushite and apatite ($p < 0.001$). Conversely, Poisson's ratios of apatite and monetite cements were not statistically different ($p = 0.40$).

3.2. Porosity

Among the three studied CPCs, brushite had the lowest porosity (13 ± 2%) (Ajaxon et al., 2015), whereas apatite and monetite cements had much higher porosities (38 ± 7% (Canal et al., 2013) and 47 ± 1%, respectively). Fig. 6 shows the elastic modulus determined by DIC as a function of type of cement and the porosity of the cements.

3.3. Phase characterization

The phase composition the three cement types was evaluated with XRD and Rietveld refinement, see Fig. 7. The main precipitated phase in the set brushite cements was brushite (approximately 80 wt%), with small amounts of unreacted ß-TCP (10 wt%), ß-CPP (6 wt%, found in the as-recived ß-TCP) and monetite (3 wt%). The monetite cements contained mainly monetite (approximately 86 wt%) with small amounts of ß-TCP and ß-CPP (7 wt% of each) after setting. The main phase in the apatite cements was hydroxyapatite (approximately 92 wt %), with small amounts of unreacted α-TCP (6 wt%) and ß-TCP (2 wt %). XRD patterns and accuracy of Rietveld refinement can be found in Figs. 8 and 9a, b and c, respectively.

4. Discussion

In this study, the compressive strength, strain-to-crack-initiation and the elastic parameters (elastic modulus and Poisson's ratio) of three different types of CPCs were determined. Different experimental approaches were used to estimate the elastic properties, including measurement of displacement (by the built-in optical encoder or LVDT) of the platens (FP or SSP) used to apply the compressive load or direct measurement of surface strains using the DIC technique.

XRD and Rietveld refinement (Fig. 7) showed that phase compositions of the brushite, monetite, and apatite cements were comparable to what has been found before for the same or similar cements (Ajaxon et al. 2015; Åberg et al. 2010).

The measured σ_{UCS} values were found to be affected by the platen type for brushite cements (Fig. 3). SSP can compensate for non-parallel ends of the specimen, a compensation not possible using FP. Therefore in the latter case, stress risers at the specimen ends may occur due to reduced contact area caused by non-parallel ends. The lower the porosity, the greater is the measured difference, due to a sensitivity to stress risers.

Stress riser effects could also explain the differences observed in σ_{CIR} and σ_{UCS} values measured using SSP (Fig. 4). In fact, either end surface micro-irregularities or defects, *e.g.* pores, within the bulk material cause localised stress concentrations. In brushite and apatite cements, this phenomenon determines the formation of cracks or even the chipping of a small part of the specimen. The specimen can still withstand

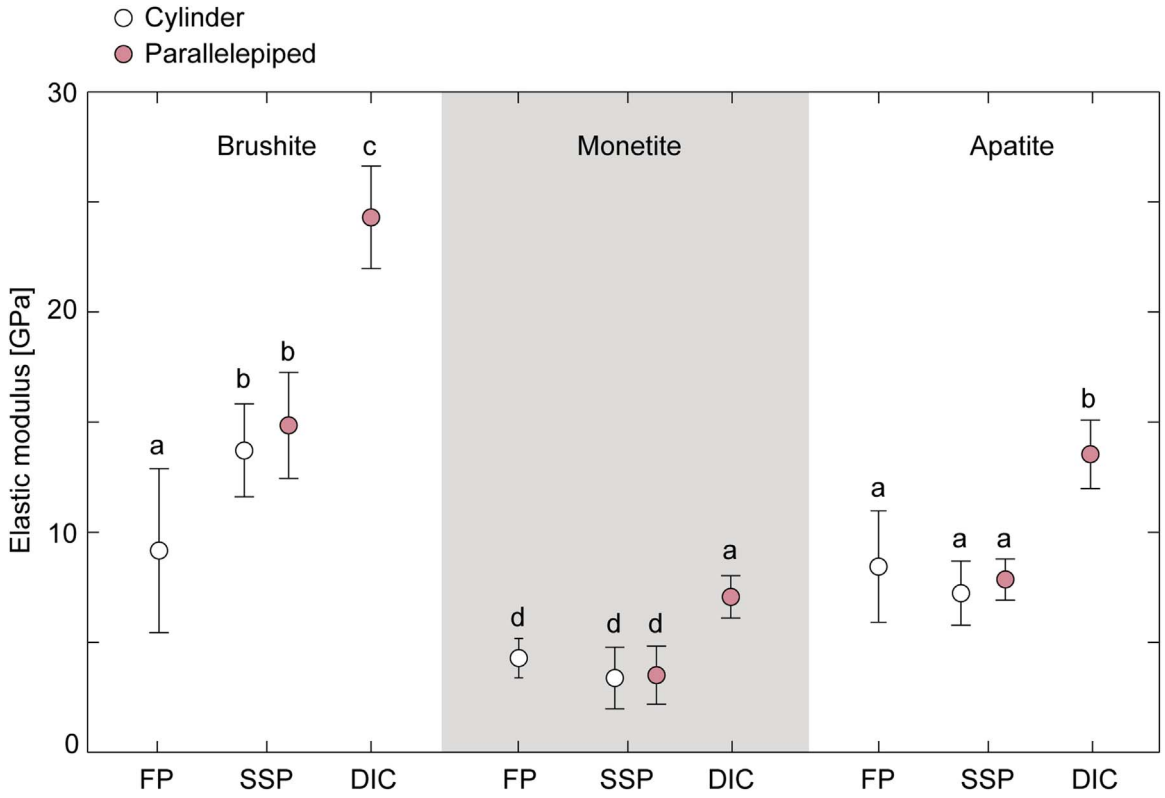

Fig. 5. Elastic modulus of brushite, monetite and apatite cements obtained from FP and SSP, as well as from the DIC-system. Error bar shows one standard deviation. Groups with the same letter are not significantly different.

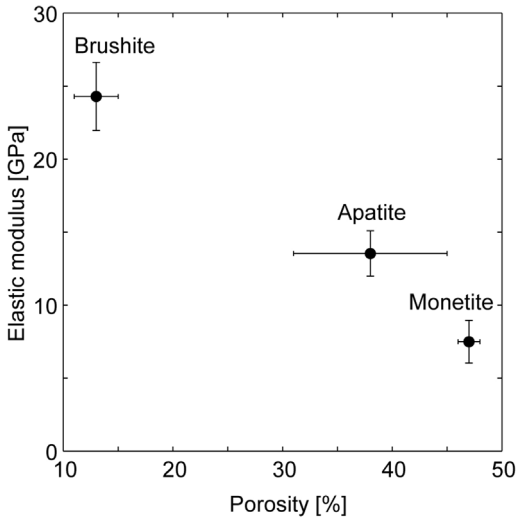

Fig. 6. Elastic modulus (from DIC) as a function of cement type and porosity.

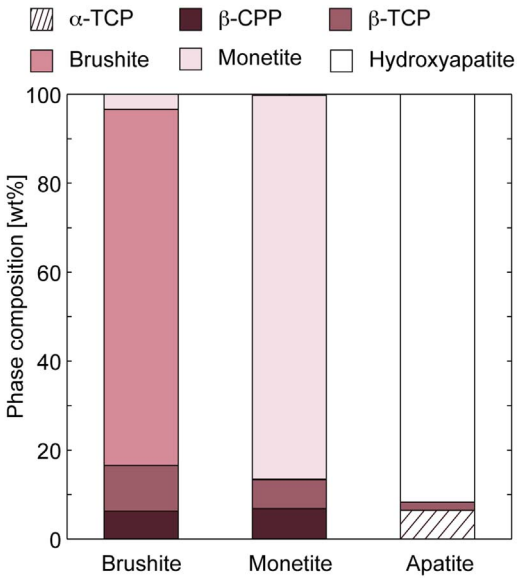

Fig. 7. Phase composition of the three types of cements. Repeatability was equal to or better than 2 wt% for (N = 6 per group).

compressive load, although its original cross-section is decreased. Indeed, the highest values of σ_{UCS} were measured when complete fracture of the specimen occurred simultaneously (3 out of 30 brushite specimens, none of the apatite specimens). A different behaviour under compressive load was observed for monetite cement. When fracture takes place, this material crumbles into small particles. Therefore, the first drop in load occurs when the specimen fractures, leading to σ_{CIR} values corresponding to σ_{UCS} values for the monetite cement. The mode of failure affects the measurement of surface strains. In fact, the ultimate strain of the cements could not be correctly determined since either crack formation led to an inhomogeneous strain distribution within the specimen, or the strain could not be measured at all when chipping occurred on the monitored surface. Instead, the strain to chipping was determined and it was found to be similar for all three cement types.

The different experimental procedures also affected the measurement of the elastic response, as expected. Significant differences in elastic moduli obtained from platen measurements and DIC were seen for all cement types. The lowest moduli (3–14 GPa) were obtained from the stress-strain curves from platen measurements (Fig. 5). Both transducers (optical encoder and LVDT) had an accuracy of ± 0.01 mm in the used range and the equipment assures high linearity for displacement. However, the accuracy of the transducers was close to the strain-to-crack-initiation (approx. 0.2% based on DIC results, *i.e.*,

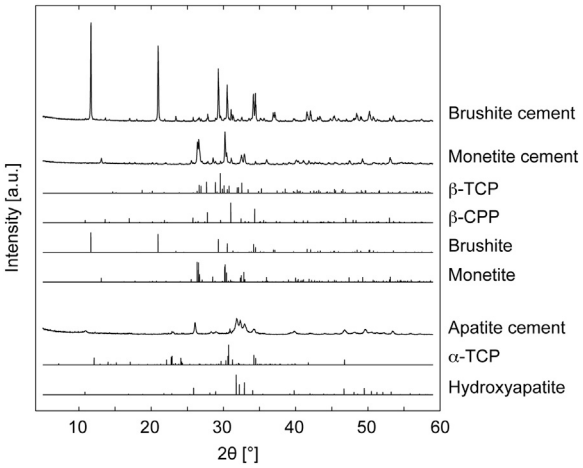

Fig. 8. XRD patterns of set brushite, monetite and apatite cements (one representative pattern out of six for each type of cement is shown) together with reference patterns for identified phases.

approx. 0.02 mm or 0.04 mm, depending on specimen geometry). Although the adoption of transducers with higher accuracy may decrease the experimental errors, it does not eliminate end artefacts leading to an underestimation of the true elastic modulus, in agreement with previous findings (Koh et al., 2014). As already mentioned, by using SSP, end artefacts can be diminished. In fact, for brushite cements higher values were obtained with this method (around 14 GPa, Fig. 5).

The highest elastic moduli were found with the DIC-system (roughly about 2 times higher compared to SSP for all cements, Fig. 5). Direct strain measurement on the specimen surface is not affected by end artefacts. It could be argued that the DIC-technique is also affected by experimental errors, depending on the quality of the speckle pattern, DIC hardware, parameters used in image-processing, and the correlation algorithm (Barranger et al., 2010; Pan, 2013; Périé et al., 2002; Rajan et al., 2012), and therefore the elastic modulus obtained using this technique might be overestimated. However, it has been demonstrated that using the appropriate procedure the DIC-technique can measure small homogeneous strain fields (< 0.1%) with accuracy better than 2% (Acciaioli et al., Submitted for publication). This means that the elastic modulus obtained by DIC could have been overestimated by up to 2% only. Therefore, the observed differences in elastic moduli should mainly be due to measuring error of the platen-

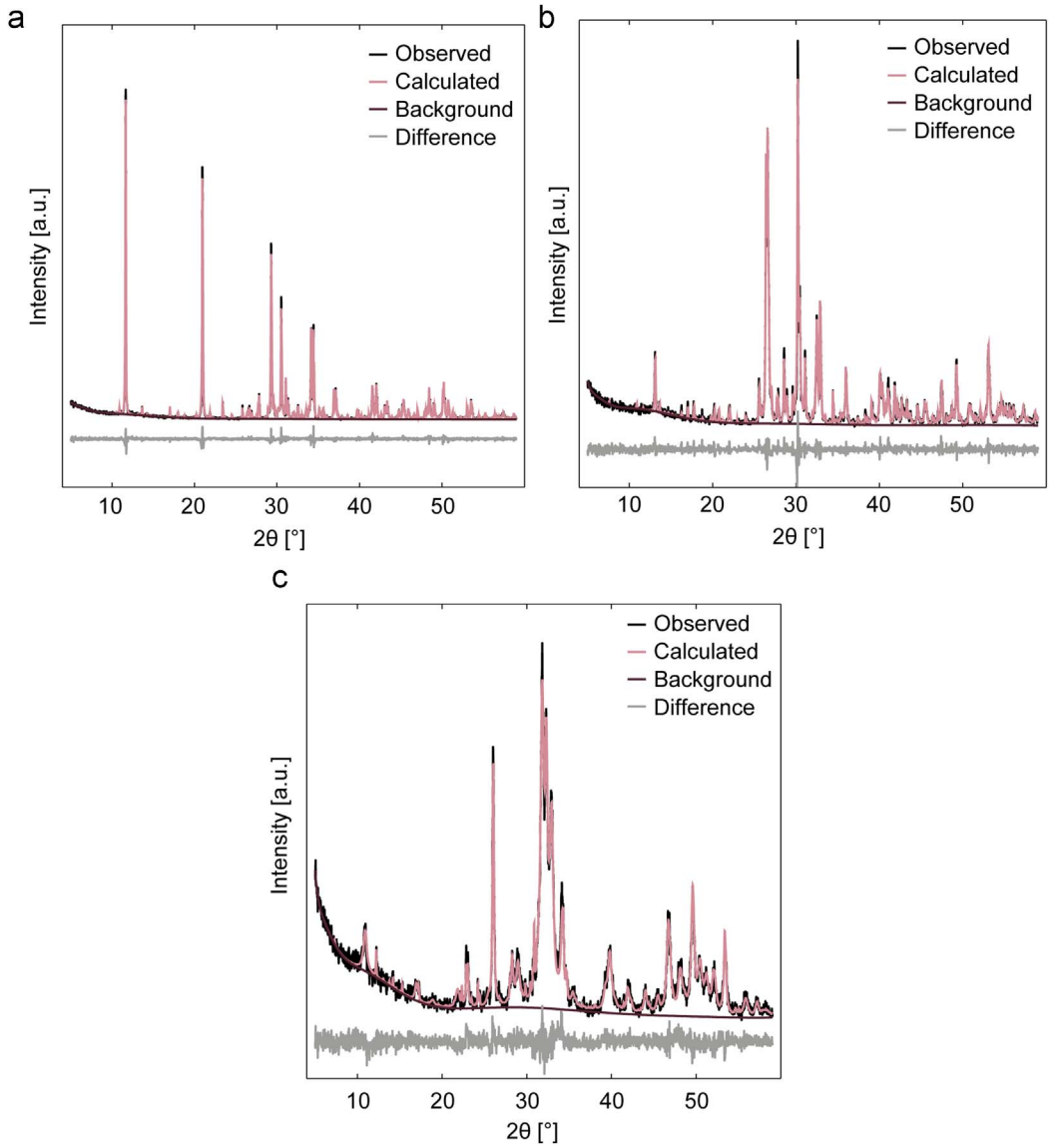

Fig. 9. Representative XRD patterns showing the accuracy of the refinement for a) brushite b) monetite and c) apatite cements.

techniques, as has been demonstrated by other authors (Koh et al., 2014).

The findings of the present study underline the importance of determining the mechanical characteristics of CPCs using an appropriate procedure, *i.e.*, using SSP and measuring deformation directly on the specimen surface, at a high enough resolution. The σ_{UCS} found under these conditions for brushite, monetite and apatite (Fig. 4) are within the range found before for the same type of materials (Table 1). Conversely, values of elastic moduli (Fig. 5) were considerably higher than the range that has previously been found for similar materials (Table 1), values that were either determined by the platen-technique or the method was not specified. The different experimental procedures used may explain a large part of the observed differences. However, variations in porosity and pore size distribution may also have a substantial effect.

The relationship between the elastic modulus and porosity of other porous materials has been reported before, revealing a decreasing modulus with increasing porosity (Rajzer et al., 2016; Rice, 1977; Soroka and Sereda, 1968). Although the porosity was not explicitly varied for each formulation, which is a limitation of the present study, the three investigated cements had substantially different porosities. Indeed, the results found herein (Fig. 6) are well in line with the above-mentioned studies. It should be noted that the porosities of the cements in the present study were evaluated by three different methods (solvent exchange, water resaturation and mercury intrusion porosimetry for brushite, monetite and apatite cements, respectively), which may give slightly different results, however not more than a few percentage points (Ajaxon et al., 2015; Engstrand Unosson et al., 2015). Other factors may naturally also be important to the results, such as crystal structure and size of the different materials, as further discussed below.

It is noteworthy that the elastic moduli (obtained by DIC, Fig. 5) for the three cement types were higher compared to the range reported in the literature for trabecular bone, and the values determined for brushite and apatite fell in the range reported for cortical bone (Table 1). As a stiffness matching that of the surrounding bone may be desired, tuning the porosity could be an approach to achieve this (while paying attention to changes in other important parameters, *e.g.*, setting time, cohesion, compressive strength, fatigue properties). On the other hand, while the quasi-static strength of the current brushite and apatite cements were higher than that of trabecular bone, it was lower than that of cortical bone (Table 1).

Porosity seemed to affect Poisson's ratio to a less extent compared to compressive strength and elastic modulus; only slight variations in Poisson's ratio were observed for the three studied CPCs. The comparison with the scarce data available in the literature must be done keeping in mind that the DIC technique used in this study tends to overestimate the Poisson's ratio up to 4% (Acciaioli et al., Submitted for publication). Poisson's ratio for the cements found in this study is similar to what has been found before for a pre-mixed apatite/chitosan cement, using an ultrasound through-transmission method (0.19–0.26 after 3–14 days in Ringer's solution) (Rajzer et al., 2016). The apatite/chitosan cement had a higher porosity (50–55%), was weaker in compression (3–5 MPa) and had a lower elastic modulus (3–5 GPa, as determined by ultrasound) compared to the cement herein. The only other study of Poisson's ratio for brushite and pure apatite cements was performed on hollow cement cylinders (Charrière et al., 2001). Poisson's ratio for monetite cements has never been presented before.

A limitation of this study is that only three specific cement formulations were investigated. The elastic properties of the materials may be substantially different depending on differences in, *e.g.*, chemical composition, particle sizes of starting powders, additives, L/P-ratio and resulting crystal shape and size. Thus, future studies should focus on evaluating the effect these parameters have on the elasticity of the cements. Also, even though the investigated CPCs represent very different porosities, the effect of porosity on the elastic parameters should be further investigated in a more systematic way by varying the porosity of each cement type by, *e.g.*, using different L/P-ratios.

To summarize, this study showed that DIC could be used to determine the elastic modulus and Poisson's ratio for brittle CPCs. An accurate knowledge of these material parameters is important when characterizing the cements, especially for computational purposes.

5. Conclusions

In this study, the DIC technique was used to estimate strains during compression of brushite, monetite and apatite cements, for the first time. The elastic moduli obtained by DIC were significantly higher (7–24 GPa) compared to those obtained from the material testers' built-in displacement measurements, whether fixed (4–9 GPa) or spherically seated (3–14 GPa) platens were used. The results confirm that previously reported values of elastic moduli of CPCs (1–8 GPa) may be substantially underestimated. Moreover, Poisson's ratio and strain-to-crack-initiation could be determined by DIC (0.20–0.26 and 0.17–0.19%, respectively). Accurate values of the elastic parameters are crucial in material development aimed at comparing the properties of different formulations and in computational models aimed to predict the material behaviour in simulated clinical scenarios.

Acknowledgement

The Swedish Foundation for International Cooperation in Research and Higher Education (STINT, project IG2011-2047), the Swedish Research Council (Project 621-2011-6258), and the Italian Program of Donation for Research "5×1000" are gratefully acknowledged for financial support. The authors are grateful to Céline Robo, Jonas Åberg, Ghanim Ibrahim, Alejandro López and Roberta Fognani for experimental support.

References

Acciaioli, A., Lionello, G., Baleani, M. Experimentally achievable accuracy using digital image correlation technique in measuring small-magnitude (< 0.1%) homogeneous strain field. Submitted for publication.

Ajaxon, I., Maazouz, Y., Ginebra, M.P., Öhman, C., Persson, C., 2015. Evaluation of a porosity measurement method for wet calcium phosphate cements. J. Biomater. Appl. 30, 526–536. http://dx.doi.org/10.1177/0885328215594293.

Ajaxon, I., Persson, C., 2017. Mechanical properties of brushite calcium phosphate cements. In: Shi, D. (Ed.), The World Scientific Encyclopedia of Nanomedicine and Bioengineering II: Bioimplants, Regenerative Medicine, and Nano-Cancer Diagnosis and Phototherapy - Volume 3: Design of Bioactive Materials for Bone Repair and Regeneration. World Scientific Pte Ltd., Singapore, pp. 285–300.

Apelt, D., Theiss, F., El-Warrak, A.O., Zlinszky, K., Bettschart-Wolfisberger, R., Bohner, M., Matter, S., Auer, J.A., Rechenberg, von, B., 2004. In vivo behavior of three different injectable hydraulic calcium phosphate cements. Biomaterials 25, 1439–1451. http://dx.doi.org/10.1016/j.biomaterials.2003.08.073.

American Society for Testing and Materials, 2015. ASTM D790-15: Standard Test Methods for Flexural Properties of Unreinforced and Reinforced Plastics and Electrical Insulating Materials. ASTM International, West Conshohocken, PA. http://dx.doi.org/10.1520/D0618.

American Society for Testing and Materials, 2014. ASTM D638-14: Standard Test Methods for Tensile Properties of Plastics. ASTM International, West Conshohocken, PA. http://dx.doi.org/10.1520/D0229.

American Society for Testing and Materials, 2013. ASTM E177-14: Standard Practise for Use of the Terms Precision and Bias in ASTM Test Methods. ASTM, West Conshohocken, PA. http://dx.doi.org/10.1520/E0456.

American Society for Testing and Materials, 2008. ASTM F 451-08: Standard Specification for Acrylic Bone Cement. ASTM, West Conshohocken, PA.

Bajammal, S.S., 2008. The use of calcium phosphate bone cement in fracture treatment a meta-analysis of randomized trials. J. Bone Jt. Surg. Am. 90, 1186–1196. http://dx.doi.org/10.2106/JBJS.G.00241.

Barralet, J.E., Hofmann, M., Grover, L.M., Gbureck, U., 2003. High-strength apatitic cement by modification withα-hydroxy acid salts. Adv. Mater. 15, 2091–2094. http://dx.doi.org/10.1002/adma.200305469.

Barranger, Y., Doumalin, P., Dupré, J.C., Germaneau, A., 2010. Digital Image Correlation accuracy: influence of kind of speckle and recording setup. EPJ Web Conf. 6, 31002. http://dx.doi.org/10.1051/epjconf/20100631002.

Bayraktar, H.H., Morgan, E.F., Niebur, G.L., Morris, G.E., Wong, E.K., Keaveny, T.M., 2004. Comparison of the elastic and yield properties of human femoral trabecular and cortical bone tissue. J. Biomech. 37, 27–35. http://dx.doi.org/10.1016/S0021-9290(03)00257-4.

Bergmann, J., Friedel, P., Kleeberg, R., 1998. BGMN - a new fundamental parameters

based rietveld program for laboratory X-ray sources, it's use in quantitative analysis and structure investigations. IUCr Comm. Powder Diffr. Newsl. no. 20, 5–8.
Bevill, G., Farhamand, F., Keaveny, T.M., 2009. Heterogeneity of yield strain in low-density versus high-density human trabecular bone. J. Biomech. 42, 2165–2170. http://dx.doi.org/10.1016/j.jbiomech.2009.05.023.
Bohner, M., Galea, L., Doebelin, N., 2012. Calcium phosphate bone graft substitutes: failures and hopes. J. Eur. Ceram. Soc. 32, 2663–2671.
Bohner, M., Gbureck, U., Barralet, J.E., 2005. Technological issues for the development of more efficient calcium phosphate bone cements: a critical assessment. Biomaterials 26, 6423–6429. http://dx.doi.org/10.1016/j.biomaterials.2005.03.049.
Boroujeni, N.M., Zhou, H., Luchini, T.J.F., Bhaduri, S.B., 2013. Development of multi-walled carbon nanotubes reinforced monetite bionanocomposite cements for orthopedic applications. Mat. Sci. Eng. C 33, 4323–4330. http://dx.doi.org/10.1016/j.msec.2013.06.029.
Boudin, S., Grandin, A., Borel, M.M., Leclaire, A., Raveau, B., 1993. Redetermination of the β-$Ca_2P_2O_7$ structure. Acta Crystallogr C. C49, 2062–2064. http://dx.doi.org/10.1107/S0108270193005608.
Cama, G., Gharibi, B., Sait, M.S., Knowles, J.C., Lagazzo, A., Romeed, S., Di Silvio, L., Deb, S., 2013. A novel method of forming micro- and macroporous monetite cements. J. Mater. Chem. B 1, 958–969. http://dx.doi.org/10.1039/c2tb00153e.
Canal, C., Pastorino, D., Mestres, G., Schuler, P., Ginebra, M.-P., 2013. Relevance of microstructure for the early antibiotic release of fresh and pre-set calcium phosphate cements. Acta Biomater. 9, 8403–8412. http://dx.doi.org/10.1016/j.actbio.2013.05.016.
Carter, J.L.W., Uchic, M.D., 2015. Impact of Speckle Pattern Parameters on DIC Strain Resolution Calculated from In-situ SEM Experiments. In: Carroll, J., Daly, S. (Eds.), Fracture, Fatigue, Failure, and Damage Evolution. Conference Proceedings of the Society for Experimental Mechanics Series. Springer, Cham, pp. 1–8. doi:10.1007/978-3-319-06977-7_16.
Charrière, E., Terrazzoni, S., Pittet, C., Mordasini, P., Dutoit, M., Lemaître, J., Zysset, P., 2001. Mechanical characterization of brushite and hydroxyapatite cements. Biomaterials 22, 2937–2945.
Curry, N.A., Jones, D.W., 1971. Crystal structure of brushite, calcium hydrogen orthophosphate dihydrate: a neutron-diffraction investigation. J. Chem. Soc. A 3725–3729. http://dx.doi.org/10.1039/j19710003725.
Dickens, B., Bowen, J.S., Brown, W.E., 1971. A refinement of the crystal structure of $CaHPO_4$ (synthetic monetite). Acta Crystallogr C. B28, 797–806. http://dx.doi.org/10.1107/S056774087200322X.
Dickens, B., Schroeder, L.W., Brown, W.E., 1974. Crystallographic studies of the role of Mg as a stabilizing impurity in β-$Ca_3(PO_4)_2$. The crystal structure of pure β-$Ca_3(PO_4)_2$. J. Solid State Chem. 10, 232–248.
Doebelin, N., Kleeberg, R., 2015. Profex: a graphical user interface for the Rietveld refinement program BGMN. J. Appl. Cryst. 48, 1573–1580. http://dx.doi.org/10.1107/S1600576715014685.
Dorozhkin, S.V., 2010. Bioceramics of calcium orthophosphates. Biomaterials 31, 1465–1485. http://dx.doi.org/10.1016/j.biomaterials.2009.11.050.
Döbelin, N., 2015. Interlaboratory study on the quantification of calcium phosphate phases by Rietveld refinement. Powder Diffr. 30, 231–241. http://dx.doi.org/10.1017/S088571561500038X.
Engstrand Unosson, J., Persson, C., Engqvist, H., 2015. An evaluation of methods to determine the porosity of calcium phosphate cements. J. Biomed. Mater. Res B 103, 62–71. http://dx.doi.org/10.1002/jbm.b.33173.
Engstrand, T., Kihlström, L., Lundgren, K., Trobos, M., Engqvist, H., Thomsen, P., 2015. Bioceramic implant induces bone healing of cranial defects. Plast. Reconstr. Surg. GlobOpen 3, e491. http://dx.doi.org/10.1097/GOX.0000000000000467.
Engstrand, T., Kihlström, L., Neovius, E., Skogh, A.-C.D., Lundgren, T.K., Jacobsson, H., Bohlin, J., Åberg, J., Engqvist, H., 2014. Development of a bioactive implant for repair and potential healing of cranial defects. J. Neurosurg. 120, 273–277. http://dx.doi.org/10.3171/2013.6.JNS1360.
Eriksen, R., Berggreen, C., Boyd, S.W., Dulieu-Barton, J.M., 2010. Towards high velocity deformation characterisation of metals and composites using Digital Image Correlation. EPJ Web Conf. 6, 31013. http://dx.doi.org/10.1051/epjconf/20100631013.
Espanol, M., Perez, R.A., Montufar, E.B., Marichal, C., Sacco, A., Ginebra, M.P., 2009. Intrinsic porosity of calcium phosphate cements and its significance for drug delivery and tissue engineering applications. Acta Biomater. 5, 2752–2762. http://dx.doi.org/10.1016/j.actbio.2009.03.011.
Gbureck, U., Spatz, K., Thull, R., Barralet, J.E., 2005. Rheological enhancement of mechanically activated α-tricalcium phosphate cements. J. Biomed. Mater. Res B 73B, 1–6. http://dx.doi.org/10.1002/jbm.b.30148.
Ginebra, M.P., Driessens, F.C.M., Planell, J.A., 2004. Effect of the particle size on the micro and nanostructural features of a calcium phosphate cement: a kinetic analysis. Biomaterials 25, 3453–3462. http://dx.doi.org/10.1016/j.biomaterials.2003.10.049.
Ginebra, M.P., 2008. Calcium phosphate bone cements. In: Deb, S. (Ed.), Orthopaedic Bone Cements. CRC Press Woodhead Publishing Limited, Cambridge, pp. 206–230.
Habibovic, P., Gbureck, U., Doillon, C., Bassett, D.C., van Blitterswijk, C.A., Barralet, J.E., 2008. Osteoconduction and osteoinduction of low-temperature 3D printed bioceramic implants. Biomaterials 29, 944–953. http://dx.doi.org/10.1016/j.biomaterials.2007.10.023.
Habraken, W.J.E.M., Zhang, Z., Wolke, J.G.C., Grijpma, D.W., Mikos, A.G., Feijen, J., Jansen, J.A., 2008. Introduction of enzymatically degradable poly(trimethylene carbonate) microspheres into an injectable calcium phosphate cement. Biomaterials 29, 2464–2476. http://dx.doi.org/10.1016/j.biomaterials.2008.02.012.
Helgason, B., Perilli, E., Schileo, E., Taddei, F., Brynjólfsson, S., Viceconti, M., 2008. Mathematical relationships between bone density and mechanical properties: a literature review. Clin. Biomech. 23, 135–146. http://dx.doi.org/10.1016/j.clinbiomech.2007.08.024.
Hofmann, M.P., Mohammed, A.R., Perrie, Y., Gbureck, U., Barralet, J.E., 2009. High-strength resorbable brushite bone cement with controlled drug-releasing capabilities. Acta Biomater. 5, 43–49. http://dx.doi.org/10.1016/j.actbio.2008.08.005.
ISO, 2002. ISO 5833: Implants for surgery — Acrylic resin cements (No. 5833).
Kaneko, T.S., Pejcic, M.R., Tehranzadeh, J., Keyak, J.H., 2003. Relationships between material properties and CT scan data of cortical bone with and without metastatic lesions. Med. Eng. Phys. 25, 445–454. http://dx.doi.org/10.1016/S1350-4533(03)00030-4.
Keaveny, T.M., Hayes, W.C., 1993. Mechanical properties of cortical and trabecular bone. [Bone] In: Hall, B.K. (Ed.), Bone Growth - B 7. CRC Press, Boca Raton, pp. 285–344.
Koh, I., López, A., Helgason, B., Ferguson, S.J., 2014. The compressive modulus and strength of saturated calcium sulphate dihydrate cements: implications for testing standards. J. Mech. Behav. Biomed. Mater. 34, 187–198. http://dx.doi.org/10.1016/j.jmbbm.2014.01.018.
Koohbor, B., Ravindran, S., Kidane, A., 2017. Experimental determination of Representative Volume Element (RVE) size in woven composites. Opt. Laser Eng. 90, 59–71. http://dx.doi.org/10.1016/j.optlaseng.2016.10.001.
Kopperdahl, D.L., Keaveny, T.M., 1998. Yield strain behavior of trabecular bone. J. Biomech. 31, 601–608.
Larsson, S., Bauer, T.W., 2002. Use of injectable calcium phosphate cement for fracture fixation: a review. Clin. Orthop. Relat. Res 395, 23–32.
Lecompte, D., Smits, A., Bossuyt, S., Sol, H., Vantomme, J., Van Hemelrijck, D., Habraken, A.M., 2006. Quality assessment of speckle patterns for digital image correlation. Opt. Laser Eng. 44, 1132–1145. http://dx.doi.org/10.1016/j.optlaseng.2005.10.004.
Lian, Q., Li, D.-C., He, J.-K., Wang, Z., 2008. Mechanical properties and *in-vivo* performance of calcium phosphate cement–chitosan fibre composite. Proc. Inst. Mech. Eng. H 222, 347–353. http://dx.doi.org/10.1243/09544119JEIM340.
Lionello, G., Cristofolini, L., 2014. A practical approach to optimizing the preparation of speckle patterns for digital-image correlation. Meas. Sci. Technol. 25, 1–9. http://dx.doi.org/10.1088/0957-0233/25/10/107001.
Lionello, G., Sirieix, C., Baleani, M., 2014. An effective procedure to create a speckle pattern on biological soft tissue for digital image correlation measurements. J. Mech. Behav. Biomed. 39, 1–8. http://dx.doi.org/10.1016/j.jmbbm.2014.07.007.
Liu, W., Zhang, J., Rethore, G., Khairoun, K., Pilet, P., Tancret, F., Bouler, J.-M., Weiss, P., 2014. A novel injectable, cohesive and toughened Si-HPMC (silanized-hydroxypropyl methylcellulose) composite calcium phosphate cement for bone substitution. Acta Biomater. 10, 3335–3345. http://dx.doi.org/10.1016/j.actbio.2014.03.009.
Mathew, M., Schroeder, L.W., Dickens, B., Brown, W.E., 1977. The crystal structure of α-Ca_3 $(PO_4)_2$. Acta Cryst. B-Struct. 33, 1325–1333.
Morgan, E.F., Keaveny, T.M., 2001. Dependence of yield strain of human trabecular bone on anatomic site. J. Biomech. 34, 569–577.
Pan, B., 2013. Bias error reduction of digital image correlation using Gaussian pre-filtering. Opt. Laser Eng. 51, 1161–1167.
Perilli, E., Baleani, M., Öhman, C., Fognani, R., Baruffaldi, F., Viceconti, M., 2008. Dependence of mechanical compressive strength on local variations in microarchitecture in cancellous bone of proximal human femur. J. Biomech. 41, 438–446. http://dx.doi.org/10.1016/j.jbiomech.2007.08.003.
Périé, J.N., Calloch, S., Cluzel, C., Hild, F., 2002. Analysis of a multiaxial test on a C/C composite by using digital image correlation and a damage model. Exp. Mech. 42, 318–328.
Pittet, C., Lemaître, J., 2000. Mechanical characterization of brushite cements: a Mohr circles' approach. J. Biomed. Mater. Res. 53, 769–780.
Pruitt, L.A., Chakravartula, A.M., 2011. Mechanics of Biomaterials. Cambridge University Press, Cambridge.
Rajan, V.P., Rossol, M.N., Zok, F.W., 2012. Optimization of digital image correlation for high-resolution strain mapping of ceramic composites. Exp. Mech. 52, 1407–1421. http://dx.doi.org/10.1007/s11340-012-9617-1.
Rajzer, I., Piekarczyk, W., Castaño, O., 2016. An ultrasonic through-transmission technique for monitoring the setting of injectable calcium phosphate cement. Mat. Sci. Eng. C 67, 20–25. http://dx.doi.org/10.1016/j.msec.2016.04.083.
Reilly, D.T., Burstein, A.H., 1975. The elastic and ultimate properties of compact bone tissue. J. Biomech. 8, 393–405.
Rice, R.W., 1977. Microstructure dependence of mechanical behaviour of ceramics. In: McCrone, R.K. (Ed.), Treatise on Materials Science and Technology. Academic Press, New York, pp. 199–381.
Siebert, T., Becker, T., Spiltthof, K., Neumann, I., Krupka, R., 2007. Error estimations in digital image correlation technique. Appl. Mech. Mater. 7–8, 265–270.
Soroka, I., Sereda, P.J., 1968. Interrelation of hardness, modulus of elasticity, and porosity in various gypsum systems. J. Am. Chem. Soc. 51, 337–340.
Sudarsanan, K., Young, R.A., 1969. Significant precision in crystal structure details: holly Springs hydroxyapatite. Acta Crystallogr C. B25, 1534–1543. http://dx.doi.org/10.1107/S0567740869004298.
Sutton, M.A., Orteu, J.J., Schreier, H., 2009. Image Correlation for Shape, Motion and Deformation Measurements. Springer Science & Business Media, New York.
Tamimi, F., Sheikh, Z., Barralet, J., 2012. Dicalcium phosphate cements: brushite and monetite. Acta Biomater. 8, 474–487. http://dx.doi.org/10.1016/j.actbio.2011.08.005.
Taut, T., Kleeberg, R., Bergmann, J., 1998. Seifert Software: the new Seifert Rietveld program BGMN and its application to quantitative phase analysis. Mater. Struct. 5, 57–66.
Unosson, J., 2014. Physical Properties of Acidic Calcium Phosphate Cements. Uppsala University, Uppsala.
Unosson, J., Engqvist, H., 2014. Development of a resorbable calcium phosphate cement with load bearing capacity. Bioceram. Dev. Appl. 4, 074. http://dx.doi.org/10.4172/2090-5025.1000074.

Xu, H.H.K., Zhao, L., Detamore, M.S., Takagi, S., Chow, L.C., 2010. Umbilical cord stem cell seeding on fast-resorbable calcium phosphate bone cement. Tissue Eng. Pt A 16, 2743–2753. http://dx.doi.org/10.1089/ten.tea.2009.0757.

Zhang, J., Liu, W., Schnitzler, V., Tancret, F., Bouler, J.-M., 2014. Calcium phosphate cements for bone substitution: chemistry, handling and mechanical properties. Acta Biomater. 10, 1035–1049. http://dx.doi.org/10.1016/j.actbio.2013.11.001.

Zhou, P., 2001. Subpixel displacement and deformation gradient measurement using digital image/speckle correlation (DISC). Opt. Eng. 40, 1613–1620. http://dx.doi.org/10.1117/1.1387992.

Åberg, J., Brisby, H., Henriksson, H.B., Lindahl, A., Thomsen, P., Engqvist, H., 2010. Premixed acidic calcium phosphate cement: characterization of strength and microstructure. J. Biomed. Mater. Res B 93B, 436–441. http://dx.doi.org/10.1002/jbm.b.31600.

Åberg, J., Engstrand, J., Engqvist, H., 2013. Influence of particle size on hardening and handling of a premixed calcium phosphate cement. J. Mater. Sci: Mater. Med. 24, 829–835. http://dx.doi.org/10.1007/s10856-013-4855-z.

Öhman, C., Baleani, M., Pani, C., Taddei, F., Alberghini, M., Viceconti, M., Manfrini, M., 2011. Compressive behaviour of child and adult cortical bone. Bone 49, 769–776. http://dx.doi.org/10.1016/j.bone.2011.06.035.